JOURNAL OF CATALYSIS 66, 335–346 (1980)

Coarsening Kinetics of Platinum Particles on Curved Oxide Substrates

TAE-MOON AHN[1] AND JOHN K. TIEN

Henry Krumb School of Mines, Columbia University, New York, New York 10027

AND

PAUL WYNBLATT

Scientific Research Staff, Ford Motor Company, Dearborn, Michigan 48121

The elevated-temperature growth of platinum particles supported on curved alumina substrates has been studied. A simple theory has been derived, and shows that when particle radii are close to the radius of curvature of this substrate, particles migrate to concave substrate sites. As a result of this migration and subsequent collisions and coalescence, initial particle growth rates may be enhanced. In addition, long-time particle coarsening by interparticle transport may be retarded, in comparison with rates of coarsening of particles on flat substrates. Experiments with platinum particles supported on alumina substrates with controlled surface curvature are described. The growth behavior of particles on these curved substrates is generally consistent with theoretical predictions.

1. INTRODUCTION

Supported metal catalysts, consisting of small catalytically active metal particles dispersed within the pores of a relatively inert, high-surface-area ceramic substrate, have found widespread use over the past several years in a variety of technological applications. One of the principal modes of deactivation of these catalysts manifests itself as growth of the metal particles. As this growth proceeds, it results in a decrease of the total active metal surface area and a concomitant decrease in total catalytic activity.

Particle growth in these systems can take place by either or both of two processes, namely: growth or coarsening by interparticle transport (*1–9*) and growth by particle migration, collision, and coalescence. These processes have been modeled in the past for the case of particles supported on *flat* substrates (*10–18*).

[1] Present address: Department of Nuclear Energy, Building No. 830, Brookhaven National Laboratory, Upton, Long Island, N.Y. 11973.

In conventional supported metal catalysts, the metal particles reside on the surface of a highly curved substrate. While the effects of substrate curvature on the processes of particle growth have been discussed previously in a qualitative manner (*16–18*), no quantitative assessment of these effects has been made to date. Thus, the purpose of the present paper is to develop a more quantitative formalism to account for the effects of substrate curvature on the process of particle migration as well as on coarsening by interparticle transport.

For comparison with the theoretical predictions, the results of experiments on model catalysts consisting of platinum particles supported on alumina substrates having controlled (sinusoidal) curvature are also presented.

2. THEORETICAL CONSIDERATIONS

A. *Effects of Substrate Curvature on Biased Particle Migration*

On flat substrates, there exists no driving force for particle migration; thus, the phe-

0021-9517/80/120335-12$02.00/0

nomenon has been treated as a random thermal process analogous to Brownian motion (*16–18*). We differentiate here between that phenomenon and particle migration on curved substrates by referring to the latter process as "biased" particle migration.

We consider first the energetics of a particle on a curved substrate. Figure 1 gives a two-dimensional section through a continuous spherical pore (substrate) with positive and negative curvatures of radius R_p. Position 1 is at the top of a convex site, or hilltop, and position 2 is at the bottom of a concave site, or valley. The energy of a particle between 1 and 2 varies with position due to the continuously changing substrate curvature. The minimum-energy configuration of a particle on an arbitrarily curved substrate may be described by the Euler equation, a free-boundary condition, and constant-volume constraints, for a given substrate morphology (*19–24*). Unfortunately, the previous solutions do not apply to particles lying at any intermediate positions between 1 and 2 in Fig. 1.

Here we simplify the problem by assuming that the shape of a particle at any position on the substrate is a segment of a sphere. It is further assumed that the total surface energy of the particle is just the metal/vapor interfacial energy. This latter assumption is justified for Pt particles supported on alumina because the difference between the Pt/Al_2O_3 and Al_2O_3/vapor interfacial energies is only 280 ergs/cm^2 (*25*), which is small compared with 2097 ergs/cm^2 for the Pt/vapor interfacial energy.

The effective radius, R_2, of a particle at position 2 may be calculated for fixed particle and pore volume, maintaining a contact angle of $\Theta = 90°$ as an equilibrium condition, by a simple geometric construction described in the Appendix. It is also possible to calculate the effective radius, R_f, of a particle of equal volume located on a flat substrate, and then plot the percentage increment of R_2 with respect to R_f as a function of R_f/R_p, as shown in Fig. 2. The functional trend of the curve in the figure shows that the effective particle radius (R_2) will increase as the particle size (defined on the flat substrate) approaches the pore size.

Similarly, we can assess the configuration of a particle at position 1, defining its effective radius as R_1 (see Fig. 1). For any degree of wetting R_1 will be less than R_f, and the difference between R_f and R_1 will be approximately equal to the difference between R_2 and R_f, R_2 being always greater than R_1.

Consider now a particle migrating downhill from position 1 to position 2. The driving force for this is the change in chemical potential which results when the effective radius of the particle increases from R_1 to R_2. The chemical potentials at positions 1 and 2 are given by:

$$\mu_1 = \mu_0 + 2\gamma\Omega/R_1, \qquad (1A)$$

$$\mu_2 = \mu_0 + 2\gamma\Omega/R_2, \qquad (1B)$$

where μ_0 is the chemical potential of an

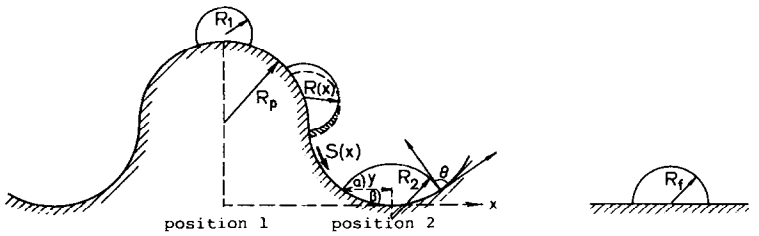

FIG. 1. Schematic of particle configurations on curved and flat substrates. Particles of radii R_1, $R(x)$, R_2, And R_f have the same volume.

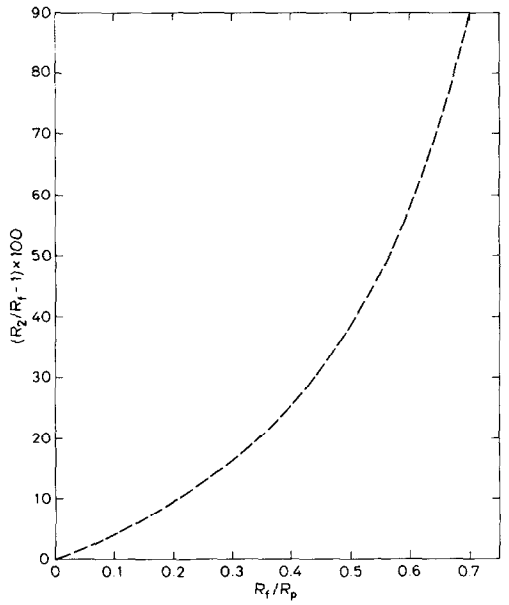

FIG. 2. The percentage increment of the radius of a particle at the bottom of a concave site with respect to the radius of the same particle on a flat substrate.

infinite-sized particle, γ is the metal/vapor interfacial energy (or surface energy), and Ω is the atomic volume of the particle material. We now assume for simplicity that the chemical potential changes linearly from μ_1 to μ_2 with particle position, x, along the substrate. Then $\mu(x)$ is given by:

$$\mu(x) = \mu_0 + 2\gamma\Omega/R_{(x)}, \quad (2)$$

where

$$R(x) = R_1/\{1 + (x/2R_p)[(R_1/R_2) - 1]\}. \quad (3)$$

In order to arrive at the rate of particle migration induced by the change in chemical potential, we adopt the methodology which has been used previously to determine the kinetics of grain boundary grooving (*27*), and the growth of holes in thin evaporated films (*28*). We further allow surface self-diffusion (of platinum over the platinum particle surface) to be the dominant mass transport mechanism. Thus, the surface diffusion flux, J_s (No. of atoms/cm·sec), which can be viewed as the flux from the trailing edge to the leading edge of the particle, is given by:

$$J_s = -[D_sC/kT][\partial\mu(x)/\partial S(x)], \quad (4)$$

where D_s is the surface diffusivity of platinum and $S(x)$ is the path length traveled and may be expressed simply as:

$$S(x) = (\pi/2)x, \quad (5)$$

and C is the atomic surface density, which is always close to 10^{15} atoms/cm^2.

The volume migration rate,

$$dv/dt = J_s\Omega[2\pi R(x)]. \quad (6)$$

The volume element dv, represented by the shaded region of the particle of radius $R(x)$ in Fig. 1, may in turn be expressed as

$$dv = [\pi R(x)/2][\pi R(x)]dS(x). \quad (7)$$

Substituting Eqs. [2]–[5] and [7] into [6], we obtain an expression for the particle migration velocity, dx/dt. Integrating x from 0 to $2R_p$, the time t_M required for the migration of a particle from position 1 to position 2 is then:

$$t_M \simeq -[(\pi^3kT)/(8D_sC\gamma\Omega^2)][\ln(R_1/R_2]/ \{(1/R_p^2)[(1/R_2) - (1/R_1)]^2\}. \quad (8)$$

The significance of each of the parameters in Eq. [8] may be clarified as follows. When temperature increases, the surface diffusivity D_s will increase exponentially, resulting in shorter t_M, and this will lead to faster particle migration. The surface energy, γ, provides the driving force for migration, and hence, higher γ will also result in faster migration. When R_p becomes very large (i.e., for nearly flat substrates), or when R_1 is equal to R_2 (i.e., for either flat substrates or little or no wetting), t_M becomes infinite or indefinite, and there is no biased particle migration. Also, the greater the difference between R_1 and R_2, the faster the migration, a condition which is fulfilled for any degree of wetting when the substrate curvature (or pore size) approaches the particle size. Finally, the smaller R_1 and R_2, the faster the ensuing migration, a result which is consistent with particle migration on flat substrates (*18*).

TABLE 1

The TIme Required for Biased Particle Migration from Convex to Concave Sites on Curved Supports at Various Temperatures[a]

T (°C)	t_M (hr)
300	6×10^{-1}
400	1.4×10^{-2}
500	9.2×10^{-4}
600	1.1×10^{-4}
700	2.2×10^{-5}
800	5.6×10^{-6}
900	1.9×10^{-6}

[a] R_p = 1 nm, R_f = 2 nm, R_2/R_1 = 1.2.

Table 1 shows values of t_M as a function of temperature from 300 to 900°C, for reasonable values of the parameters. Here, we have used the platinum value for D_s ($0.014 \exp\{-15{,}000/T\}$ cm²/sec) (*29*), and $C\Omega^2 = (2^{1/2}a^4)/(8(3)^{1/2})$ appropriate for a (111) fcc surface, where a is the lattice parameter. The pore size and particle size have been taken to be R_p = 10 nm and R_f = 2 nm, respectively. Thus, $R_2/R_f \simeq 1.1$ (from Fig. 2) and $R_2/R_1 \simeq 1.2$. The resulting magnitudes of t_M are all rather short (less than 1 hr) in comparison with catalyst lifetimes.

Once the process of particle migration is complete, particles which have arrived at the same concave site in the substrate will presumably collide and coalesce, leading to particle growth. However, no further growth by this process is likely since particles will tend to be trapped at concave sites by the chemical potential barrier confronting migration out of a concave site. The actual extent of particle growth resulting from this process, in a conventional catalyst, may vary from large to insignificant depending on the number of particles which are initially present within a given pore (or topological catchment area), i.e., depending on the particle areal density as well as on the pore size.

B. Effects of Substrate Curvature on Growth by Interparticle Transport

As we have seen in the previous section, when particles reside on substrates having curvatures comparable with the particle curvature, rapid migration of the particles from convex to concave regions of the substrate can take place. Thus, when considering the effect of substrate curvature on particle coarsening by interparticle transport, we only need be concerned with growth of particles residing in concave sites.

We calculate first the rate of increase (or decrease) of the exposed surface area, A, of a particle with volume V, existing within a distribution of particles. We also define the volume of the particle which is neither growing nor shrinking within the distribution, at any given time, as V^*. Second, for purposes of comparison, we calculate the rate of increase (or decrease) of the exposed surface area of a particle of volume V residing on a flat substrate. In this treatment, consideration of volumes rather than radii is necessary because the effective radius, R_2 (or R_1), of a particle (see Fig. 1) in the presence of substrate curvature, no longer represents the inverse of the exposed surface area of the particle.

The volume change of a particle by interparticle transport, either on a concave or on a flat substrate, may generally be written as:

$$dV/dt = J\Omega, \tag{9}$$

where J (No. of atoms/sec) is the atomic current arriving at or leaving the exposed surface area of a particle. Hence, the rate of change of surface area is:

$$dA/dt = J\Omega(dA/dV). \tag{10}$$

Expressions for (dA/dV) for flat and curved substrates are given in the Appendix. J has been derived in the past for flat substrates in terms of particle radii (*17, 18*). In the present treatment, J is rearranged in terms

of V, V^*, the pore volume, V_p, and the contact angle, θ.

In the limit of substrate diffusion control, for curved substrates, the rate of change of R_2 is given by:

$$\frac{dR_2}{dt} = \frac{4K_D}{(2 - 3\cos\alpha + \cos^3\alpha)} \frac{1}{R_2^3}\left(\frac{R_2}{R_2^*} - 1\right), \quad (11)$$

where (*10*)

$$K_D = \frac{a^2\gamma\Omega^2 P_{O_2} K_{eq}}{kT(2\pi MkT)^{1/2}} \exp\{-(H_m^s - H_{sv})/kT\},$$

P_{O_2} is oxygen partial pressure, K_{eq} is the equilibrium constant for the reaction $Pt + O_2 \rightleftarrows PtO_2$, M is the molecular weight of PtO_2, H_m^s is the migration energy of the PtO_2 molecule on the substrate, H_{sv} is the energy required to transfer the molecule from the substrate to the vapor phase, R_2^* is the radius of a particle having volume V^*, and α is a geometric parameter defined in Fig. 1. The flux is then:

$$J(V, V^*, V_p, \theta) = (1/\Omega)(4\pi R_2^2)(1/4)(2 - 3\cos\alpha + \cos^3\alpha)\cdot\left(\frac{dR_2}{dt}\right). \quad (12)$$

Substituting Eq. [11] into Eq. [12] and using the results of the Appendix, the flux becomes:

$$J(V, V^*, V_p, \theta) = (1/\Omega)(4\pi K_D)\cdot(1/y^*p^* - 1/yp), \quad (13)$$

where y^* and p^* are the values of geometric parameters y and p of the particle of volume V^*. For flat substrates the expression is:

$$J(V, V^*, \theta) = (1/\Omega)(4\pi R_f^2\cdot\epsilon_1)\left(\frac{dR_f}{dt}\right) = (1/\Omega)(4\pi K_D)\cdot\left(\frac{1}{R_f^*} - \frac{1}{R_f}\right) = (1/\Omega)(4\pi K_D)\cdot\left(\frac{3}{4\pi\epsilon_1}\right)^{-1/3} V^{-1/3}[(V/V^*)^{1/3} - 1] \quad (14)$$

where R_f^* is the value of R_f for the particle of volume V^* and ϵ_1 is as defined in the Appendix. Similarly, in the limit of vapor-phase diffusion for curved substrates, the flux is given by:

$$J(V, V^*, V_p, \theta) = A\cdot[1/(2\ MkT)^{1/2}](2\gamma\Omega P_{O_2} K_{eq}/kT)(1/R_2^* - 1/R_2) = [(2\gamma\Omega P_{O_2}\cdot K_{eq})/kT(2\pi MkT)^{1/2}]\cdot 2\pi y^2(p - H_p)(1/y^*\cdot p^* - 1/y\cdot p). \quad (15)$$

For flat substrates the flux is:

$$J(V, V^*, \theta) = A[2\gamma\Omega P_{O_2}\cdot K_{eq}/kT(2\ MkT)^{1/2}](1/R_f^* - 1/R_f) = [2\gamma\Omega P_{O_2}\cdot K_{eq}/kT(2\pi MkT)^{1/2}](4\pi\epsilon_2)\cdot(3/4\pi\epsilon_1)^{-1/3}V^{-1/3}[(V/V^*)^{1/3} - 1]. \quad (16)$$

The expressions for (dA/dV), given in the Appendix, may be combined with Eqs. [13]–[16] to obtain the dimensionless ratio $(dA/dt)_c/(dA/dt)_f$, where $(dA/dt)_c$ and $(dA/dt)_f$ are the rate of change of the exposed surface area of particles in concave sites or on flat substrates, respectively. This dimensionless quantity was calculated numerically as a function of $(V/V^*)^{1/3}$ and (V^*/V_p), where $(V/V^*)^{1/3}$ represents an effective dimensionless particle size, while (V^*/V_p) represents the ratio of particle volume to pore volume. Calculated values of $(dA/dt)_c/(dA/dt)_f$ (at $\theta = 90°$) for the two possible modes of interparticle transport (*17, 18*), i.e., substrate diffusion and vapor-phase diffusion, are given in Figs. 3 and 4, respectively. The figures show that as $(V/V^*)^{1/3}$, or (V^*/V_p), approaches zero, the quantity $[dA/dt)_c/(dA/dt)_f]$ approaches unity; those conditions represent the limit of vanishing substrate curvature. The figures also show that there is a strong retardation of interparticle transport as a result of substrate curvature, and that this retardation increases as particle volume approaches pore volume. It should be pointed out that the retardation of growth is a consequence of the assumption that all

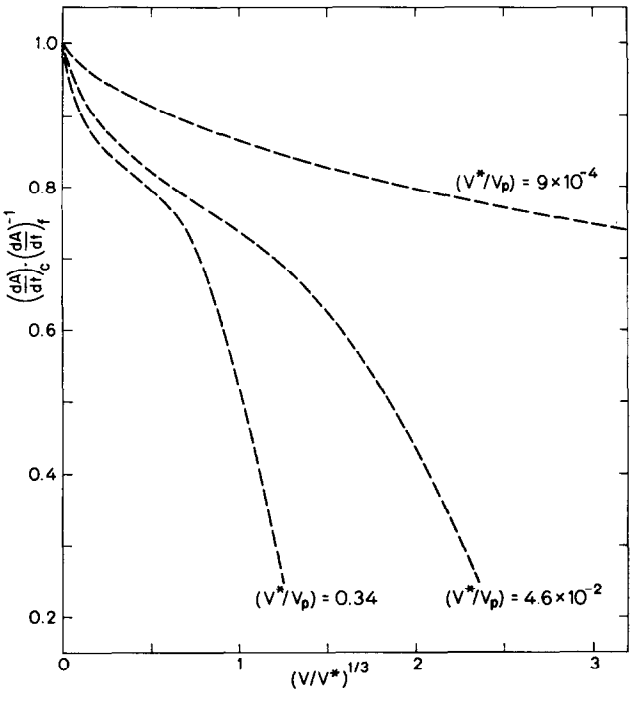

FIG. 3. Plot of dimensionless rate of surface area change of a particle at a concave site versus dimensionless particle size for the case of "noninhibited" coarsening where interparticle transport is by substrate diffusion.

particles are present in concave sites on the substrate; under those conditions the curvature (and hence the chemical potential) of a particle of given volume will be smaller in a concave site than on a flat substrate. Finally, it is interesting that, in contrast to the case of flat substrates, growth by interparticle transport is dependent on particle volume. The above results will also hold, in a general sense, in the case of "nucleation-inhibited" coarsening (*10–14*) because the effects arise mainly from geometric considerations.

A test of these predictions was attempted in the experiments described in the next section.

2. EXPERIMENTAL STUDY OF PLATINUM PARTICLES SUPPORTED ON CURVED SUBSTRATES

A. Experimental Procedure

Single-crystal alumina (sapphire) of 99.99% purity, having a (0001) surface orientation, was used as the substrate material. The technique used to produce a sinusoidal grating, or ripples, on the surface of the crystals was a modification of ion-beam micromachining processes used in the fabrication of integrated optics components (*30–32*). Briefly, the procedure was as described below.

Masks for the production of the gratings were made by exposing a photographic plate to interference patterns from an argon laser beam. A photoresist material was applied to the precleaned sapphire, exposed to ultraviolet radiation through a mask, and developed, leaving a corrugated coating on the substrate. The coated crystals were then exposed to an argon beam in an ion micromilling instrument. In order to make the grating smoother and closer to a sinusoidal shape, the samples were annealed at 1300°C for 15 to 30 min.

Gratings of 1000- and 2000-nm wavelength were made (attempts to produce

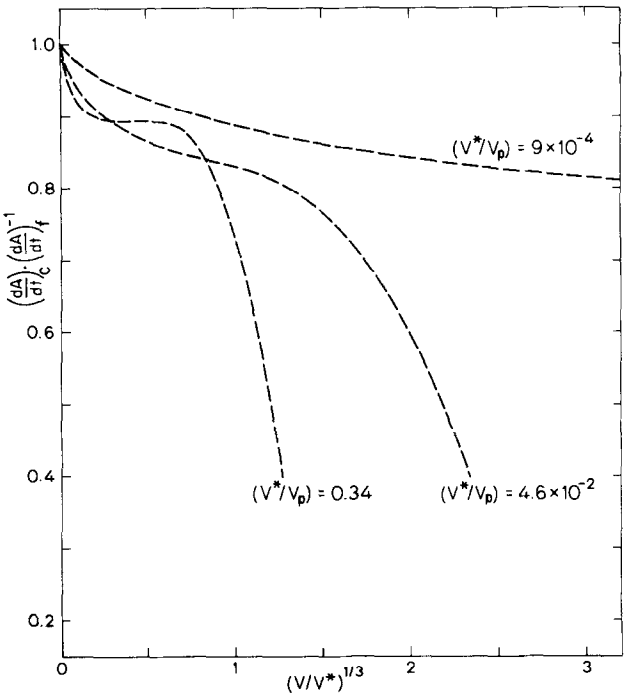

FIG. 4. Plot of dimensionless rate of surface area change of a particle at a concave site versus dimensionless particle size taken for the case of "noninhibited" coarsening where interparticle transport is by vapor-phase diffusion.

finer gratings were unsuccessful), and the approximate depth of the corrugations was measured from stereopair images obtained with a scanning electron microscope (*33*). The depth of the gratings was approximately one-tenth of the grating wavelength, equivalent to substrate radii of curvature of 250 and 500 nm, respectively.

The finished gratings were then cleaned and a thin film of platinum was deposited onto the curved surfaces by ratio-frequency sputtering. The platinum film was broken up into discrete particles by heat treating at 1000°C for 24 hr. The initial particle sizes produced on these samples were rather large, about 100 to 250 nm, but this was necessary in order to make the particle radii comparable to the smallest substrate radii of curvature achieved in the gratings. Particle size measurements were performed either by transmission electron microscopy on replicas of the surface or by scanning electron microscopy.

After film breakup, samples were heat treated either at 900 or 1100°C in 1 atm air at ambient temperatures in sealed Vycor tubes. Only the latter samples were used for quantitative particle size determinations. A particular area of the sample was selected for the initial average particle size measurements, and this same area was used in subsequent measurements after sample heat treatment.

B. Experimental Results and Discussion

Figure 5 shows the microstructures obtained with particles of radius about 250 nm, distributed on 1000- and 2000-nm-wavelength substrates, after heat treatment at 900°C for 192 and 24 hr, respectively. On the 1000-nm-wavelength substrate, the particles appear to be aligned along the valleys, whereas the distribution of particles appears to be more random on the 2000-nm-wavelength substrate. A confirmation of particle alignment was obtained by count-

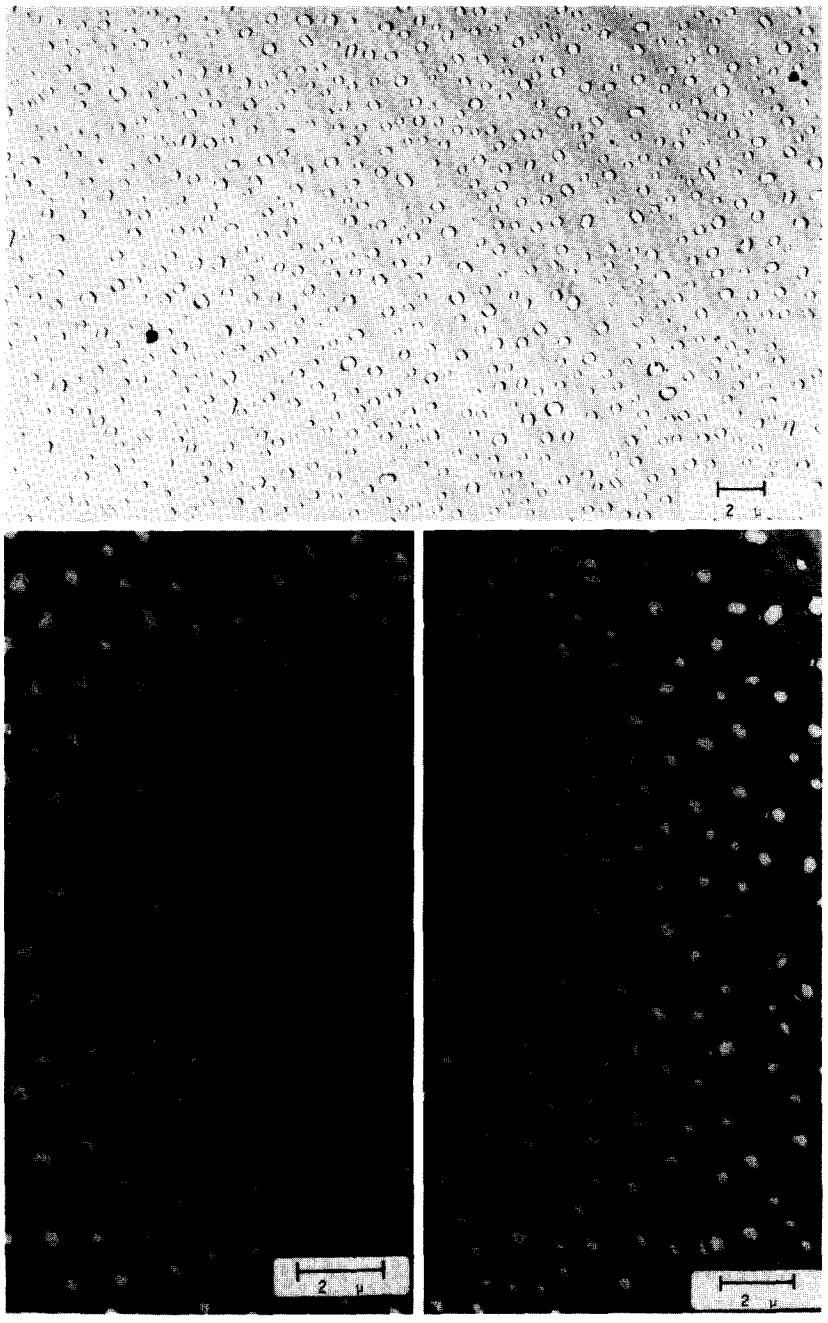

FIG. 5. Particle distributions after heat treating for 24 hr at 900°C on 2000-nm-wavelength substrate (upper) and for 192 hr at 900°C on 1000-nm-wavelength substrate (lower).

ing the number of particles lying along valleys and along lines inclined at 45 and 90° to the valleys. In the case of the 1000-nm-wavelength substrate, the number of particles lying along valleys was larger than that along other directions by a factor $\simeq 1.3$, whereas this factor was unity for the 2000-nm-wavelength substrate. This result pro-

TABLE 2

Experimentally Observed Particle Size Changes at 1100°C, and Comparison with Particles Supported on Flat Polycrystalline Substrates

Substrate	$\bar{R}(0)$ (nm)	Time (hr)	$\bar{R}(t)$ (nm)	$\bar{R}(t)/\bar{R}(0)$	Comparison with flat polycrystalline substrates[a]
1000 nm	78.1	16.5	136.2	1.74	$\bar{R}(t) \gg \bar{R}(t)_{\text{flat}}$
2000 nm	84.9	16.5	111.8	1.32	$\bar{R}(t) \geq \bar{R}(t)_{\text{flat}}$
Flat single crystal	119.8	20.0	158.0	1.32	$\bar{R}(t) \geq \bar{R}(t)_{\text{flat}}$

[a] From Ref. (*14*).

vides clear evidence of the migration of particles over the substrate from convex to concave sites. In addition, the observation that migration of particles is favored by higher substrate curvature and longer heat treatment times is qualitatively consistent with the trends by the formalism developed in Section 1A.

In Table 2 we compare the growth, or total coarsening kinetics, at 1100°C for particles supported on both types of curved substrate with coarsening kinetics of particles growing on a flat sapphire substrate. We also give a more qualitative comparison with previously determined coarsening kinetics for particles having the same initial size but supported on flat polycrystalline alumina substrates (*14*). As can be seen, over the 16.5-hr time period of the experiment, the kinetics of growth are significantly faster on the 1000-nm-wavelength substrate than on the flat substrate, whereas the rate of growth on the 2000-nm-wavelength substrate is close to that for the flat substrate.

To assess the results further, we calculate the time, t_M (see Eq. [8]), for particles to migrate to concave sites. By comparing t_M with the heat treatment time, we can estimate whether there was sufficient time for particle migration to occur.

We consider first the case of the 1000-nm-wavelength substrate. For the present experimental conditions, R_p of Eq. [8] is equivalent to one-quarter of the wavelength of the substrate. If R_f is chosen to be the average effective initial radius, $\bar{R}(0)$ in Table 2, then R_f/R_p lies between 0.3 and 0.4, which corresponds to a 15 to 25% increment in $[R_2/R_f - 1]$ (see Fig. 2), and thus to an increment of 30 to 50% in $[R_2/R_1 - 1]$. Also, because the ratio of depth to wavelength of the curved substrate is smaller by a factor of 10 than the ratio in the ideal case of Fig. 1, and the distance between positions 1 and 2 is half the wavelength, the actual increment of $[R_2/R_1 - 1]$ in this experiment is reduced by a factor of 5, yielding an increment of $[R_2/R_1 - 1]$ in the range from 6 to 10%. As shown in Fig. 6, the calculated times t_M at values of R_2/R_1 ranging from 1.05 to 1.10, and R_1/R_p values from 0.3 to 0.4, are less than 10 hr. Thus, for the 1000-nm-wavelength substrate, t_M is less than the experimental heat treatment time, and sufficient time was available for particles to migrate to valleys.

For the case of the 2000-nm wavelength substrate, we can conclude that t_M would be 16 times longer than for the 1000-nm-wavelength substrate, because both R_p and $(R_2 - R_1)$ in Eq. [8] are twice as large in this case. Accordingly, it appears consistent that we observed neither an increased number of particles in the concave sites nor an enhancement of growth in this case.

In the experiments on curved substrates, we observed either an enhancement of the particle growth rate or an equivalent growth rate, as compared with flat substrate samples. Thus, the retardation of

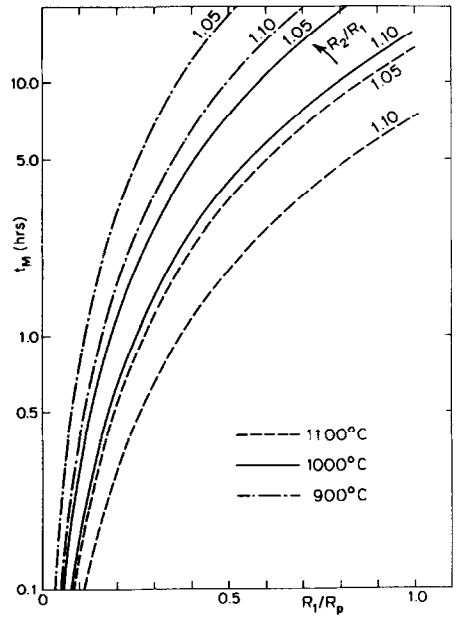

FIG. 6. Time required for biased particle migration from convex to concave sites versus the ratio of particle radius to substrate pore radius at various temperatures and wetting conditions.

growth predicted for curved substrates, when coarsening is controlled by interparticle transport, was not observed here. This result is actually consistent with the conditions prevailing in our experiments. In the case of the experiment on the 2000-nm-wavelength substrate, the substrate curvature was too mild to have any significant effect on particle growth kinetics. This conclusion is consistent with the absence of particle migration to valleys in that case, stemming from the relatively short time of the experiment in comparison with particle migration times. Thus, in this instance, we would expect growth behavior to parallel that on flat substrates, as is indeed observed.

In the case of the experiment with 1000-nm-wavelength substrate, most of the experimental period was consumed by migration of particles to valleys, and the observed enhancement is considered to reflect growth due to interparticle encounters and subsequent coalescence within the valley regions.

3. CONCLUSIONS AND INFERENCES WITH RESPECT TO CONVENTIONAL CATALYSTS

When substrate curvature is comparable to particle curvature, enhanced (and biased rather than random) migration of particles will occur toward concave regions of the substrate. If several particles migrate toward the same concave region of the substrate, then rapid growth can occur as a result of interparticle collisions and coalescence. The particles in concave regions will tend to be trapped at those locations by a chemical potential barrier opposing migration to less concave regions. However, these particles would coarsen more slowly by interparticle transport processes than particles of equal volume supported on flat substrates, because of their lower surface curvature and chemical potential. With regard to conventional supported metal catalysts, the enhanced particle migration would lead to rapid surface area loss, but the details of such loss would depend on both particle area density and pore size. For cases where those parameters are such that a pore is occupied on average by one particle or less, no significant area loss would be expected from interparticle collision or coalescence. However, even in that instance, some measurable surface area loss could result from changes in particle configuration accompanying the migration of particles from convex to concave regions of the substrate.

APPENDIX: GEOMETRIC CONSTRUCTION FOR FIG. 1

For curved substrates,

$$\alpha + \beta + \Theta = \pi \qquad \text{for } 0 \le \alpha \le \pi/2,$$

we define dimensionless quantities:

$$T_B(y, R_p) \equiv \tan \beta = (y/R_p)(1 - y^2/R_p^2)^{-1/2},$$

$$H_R(y, R_p) \equiv (1 - y^2/R_p^2)^{1/2},$$

$$H_p(y, R_p, \Theta) \equiv (T_B \cdot \tan \Theta - 1)(T_B + \tan \Theta)^{-1},$$

$$p(y, R_p, \Theta) \equiv (1 + H_p^2)^{1/2}.$$

Then

$$R_2(y, R_p, \Theta) = y \cdot p,$$

$$V(y, R_p, \Theta) = (\pi/3)R_p^3[(y/R_p)^3(p - H_p)^2 (2p + H_p) + (1 - H_R)^2(2 + H_R)],$$

$$A(y, R_p, \Theta) = 2\pi y^2(p^2 - p \cdot H_p),$$

$$\frac{dA}{dV}(y, R_p, \Theta) = \left(\frac{\partial A}{\partial y}\right)\left(\frac{\partial y}{\partial v}\right) + \left(\frac{\partial A}{\partial R_p}\right)\left(\frac{\partial R_p}{\partial V}\right) + \left(\frac{\partial A}{\partial \Theta}\right)\left(\frac{\partial \Theta}{\partial V}\right).$$

For flat substrates, we define

$$\epsilon_1 \equiv (\tfrac{1}{4})(2 + 3\cos\Theta - \cos^3\Theta),$$

$$\epsilon_2 \equiv (\tfrac{1}{2})(1 + \cos\Theta).$$

Then

$$V(R_f, \Theta) = (4\pi/3)\epsilon_1 R_f^3,$$

$$A(R_f, \Theta) = 4\pi\epsilon_2 R_f^2,$$

$$\frac{dA}{dV}(R_f, \Theta) = \left(\frac{\partial A}{\partial R_f}\right)\left(\frac{\partial R_f}{\partial V}\right) + \left(\frac{\partial A}{\partial \Theta}\right)\left(\frac{\partial \Theta}{\partial V}\right).$$

Introducing hemispherical pore volume

$$V_p = (2\pi/3)R_p^3,$$

using the parameter y and considering that $V(y, R_p, \Theta)$ is equal to $V(R_f \cdot \Theta)$ in the calculation,

$$R_2(y, R_p, \Theta) = R_2(R_f, R_p, \Theta)$$

shown in Fig. 2,

$$\frac{dA}{dV}(y, R_p, \Theta) = \frac{dA}{dV}(V, V_p, \Theta)$$

shown in Figs. 3 and 4,

$$\frac{dA}{dV}(R_f, \Theta) = \frac{dA}{dV}(V, V_p, \Theta)$$

shown in Figs. 3 and 4.

ACKNOWLEDGMENT

This work is part of a program made possible by the Division of Materials Research, National Science Foundation, under Grant NSF-DMR74-13585.

REFERENCES

1. Greenwood, G. W., *Acta Metall.* **4,** 243 (1956).
2. Lifshitz, I. M., and Slyozov, V. V., *J. Phys. Chem. Solids* **19,** 35 (1961).
3. Wagner, C., *Z. Elektrochem.* **65,** 243 (1961).
4. Chakraverty, B. K., *J. Phys. Chem. Solids* **28,** 2401 (1967).
5. Chakraverty, B. K., *J. Phys. Chem. Solids* **28,** 2413 (1967).
6. Ardell, A. J., *Acta Metall.* **20,** 601 (1972).
7. Kirchner, H. O. K., *Metall. Trans.* **2,** 2867 (1971).
8. Geguzin, Y. E., Kaganovsky, Y. S., and Slyozov, V. V., *J. Phys. Chem. Solids* **30,** 1173 (1969).
9. Slyozov, V. V., *Sov. Phys. Solid State* **9,** 927 (1967).
10. Wynblatt, P., and Gjostein, N. A., *Acta Metall.* **24,** 1165 (1976).
11. Wynblatt, P., *Acta Metall.* **24,** 1175 (1976).
12. Ahn, T. M., and Tien, J. K., *J. Phys. Chem. Solids* **37,** 771 (1976).
13. Ahn, T. M., Purushothaman, S., and Tien, J. K., *J. Phys. Chem. Solids* **37,** 777 (1976).
14. Ahn, T. M., Wynblatt, P., and Tien, J. K., submitted for publication.
15. Clark, R. W., Wynblatt, P., and Tien, J. K., to be published.
16. Wynblatt, P., Dalla Betta, R. A., and Gjostein, N. A., *in* "The Physical Basis for Heterogeneous Catalysis" (E. Drauglis and R. I. Jaffee, Eds.), p. 510. Plenum, New York, 1975.
17. Wynblatt, P., and Ahn, T. M., *in* "Materials Science Research," Vol. 10 (G. C. Koczynski, Ed.), p. 83. Plenum, New York, 1975.
18. Wynblatt, P., and Gjostein, N. A., *Progr. Solid State Chem.* **9,** 21 (1975).
19. Landau, L. D., Coll. "On the 70th Birthday of Academian" (A. F. Joffe, Ed.), p. 44 (translated from Russian).
20. Frenkel, I. I., *Exp. Theor. Phys.* **7,** 659 (1948).
21. Cahn, J. W., and Hoffman, D. W., *Acta Metall.* **22,** 1205 (1974).
22. Winterbottom, W. L., *Acta Metall.* **15,** 303 (1967).
23. Lee, J. K., and Aaronson, H. I., *Acta Metall.* **23,** 799 (1975).
24. Lee, J. K., and Aaronson, H. I., *Acta Metall.* **23,** 809 (1975).
25. McLean, M., and Hondros, E. D., *J. Mater. Sci.* **6,** 19 (1971).
26. "Standard Mathematical Tables," 19th ed., p. 17. Chem. Rubber Co., Cleveland, 1971.
27. Shewmon, P. G., "Diffusion in Solids," p. 182. McGraw–Hill, New York, 1963.
28. Brandon, R., and Bradshaw, F. J., Royal Aircraft Establishment Technical Report 66095 (1966).
29. Melmed, A. J., *J. Appl. Phys.* **41,** 1885 (1967).
30. Garvin, H. L., Garmire, E., Somekh, S., Stoll,

H., and Yariv, A., *Appl. Optics* **12,** 455 (1973).
31. Schinke, D. P., Smith, R. G., Spencer, E. G., and Galvin, M. F., *Appl. Phys. Lett.* **21,** 494 (1972).
32. Dakss, M. L., Kuhn, L., Heidrich, P. F., and Scott, B. A., *Appl. Phys. Lett.* **16,** 523 (1970).
33. Howell, P. G. T., and Boyde, A., *in* "Proceedings of the 5th Annual SEM Symposium," p. 233. IIT Research Institute, Chicago, 1972.